LETTER

https://doi.org/10.1038/s41586-018-0064-8

LUBAC is essential for embryogenesis by preventing cell death and enabling haematopoiesis

Nieves Peltzer[1,9], Maurice Darding[1,9], Antonella Montinaro[1], Peter Draber[1,2], Helena Draberova[1,2], Sebastian Kupka[1], Eva Rieser[1], Amanda Fisher[3], Ciaran Hutchinson[4], Lucia Taraborrelli[1], Torsten Hartwig[1], Elodie Lafont[1], Tobias L. Haas[5], Yutaka Shimizu[1], Charlotta Böiers[1], Aida Sarr[1], James Rickard[6,7], Silvia Alvarez-Diaz[6,7], Michael T. Ashworth[4], Allison Beal[8], Tariq Enver[1], John Bertin[8], William Kaiser[3], Andreas Strasser[6,7], John Silke[6,7], Philippe Bouillet[6,7] & Henning Walczak[1]*

The linear ubiquitin chain assembly complex (LUBAC) is required for optimal gene activation and prevention of cell death upon activation of immune receptors, including TNFR1[1]. Deficiency in the LUBAC components SHARPIN or HOIP in mice results in severe inflammation in adulthood or embryonic lethality, respectively, owing to deregulation of TNFR1-mediated cell death[2–8]. In humans, deficiency in the third LUBAC component HOIL-1 causes autoimmunity and inflammatory disease, similar to HOIP deficiency, whereas HOIL-1 deficiency in mice was reported to cause no overt phenotype[9–11]. Here we show, by creating HOIL-1-deficient mice, that HOIL-1 is as essential for LUBAC function as HOIP, albeit for different reasons: whereas HOIP is the catalytically active component of LUBAC, HOIL-1 is required for LUBAC assembly, stability and optimal retention in the TNFR1 signalling complex, thereby preventing aberrant cell death. Both HOIL-1 and HOIP prevent embryonic lethality at mid-gestation by interfering with aberrant TNFR1-mediated endothelial cell death, which only partially depends on RIPK1 kinase activity. Co-deletion of caspase-8 with RIPK3 or MLKL prevents cell death in *Hoil-1*$^{-/-}$ (also known as *Rbck1*$^{-/-}$) embryos, yet only the combined loss of caspase-8 with MLKL results in viable HOIL-1-deficient mice. Notably, triple-knockout *Ripk3*$^{-/-}$*Casp8*$^{-/-}$*Hoil-1*$^{-/-}$ embryos die at late gestation owing to haematopoietic defects that are rescued by co-deletion of RIPK1 but not MLKL. Collectively, these results demonstrate that both HOIP and HOIL-1 are essential LUBAC components and are required for embryogenesis by preventing aberrant cell death. Furthermore, they reveal that when LUBAC and caspase-8 are absent, RIPK3 prevents RIPK1 from inducing embryonic lethality by causing defects in fetal haematopoiesis.

To determine the physiological role of HOIL-1, we generated HOIL-1-deficient mice by targeting exons 1 and 2 of the *Hoil-1* (also known as *Rbck1*) gene (Extended Data Fig. 1a–d). No mice with homozygous deletion in the *Hoil-1* gene were weaned (Fig. 1a). Analysis of *Hoil-1*$^{-/-}$ embryos revealed that they died around embryonic day (E) 10.5 (Fig. 1a, b). This result was confirmed with a strain generated from an independently targeted embryonic stem (ES) cell (C20*Hoil-1*$^{-/-}$ mice) (Extended Data Fig. 1e, f). At E10.5, *Hoil-1*$^{-/-}$ embryos presented with disrupted vascular architecture and cell death in the yolk sac endothelium (Fig. 1c, d and Extended Data Fig. 1g, h), indicating that the absence of HOIL-1 causes aberrant endothelial cell death. *Hoil-1*$^{fl/fl}$*Tie2-cre*$^{+}$ embryos that lack HOIL-1 specifically in endothelial and some haematopoietic cells also died around E10.5 with the same abnormalities (Fig. 1e and Extended Data Fig. 1i, j). Loss of TNF or TNFR1 diminished cell death in the yolk sac and prevented lethality at E10.5 in *Hoil-1*$^{-/-}$ embryos (Fig. 1f and Extended Data Fig. 2a–d). As in the *Tnfr1*$^{-/-}$*Hoip*$^{-/-}$ (also known as *Tnfrsf1a*$^{-/-}$*Rnf31*$^{-/-}$) double knockouts[8], *Tnfr1*$^{-/-}$*Hoil-1*$^{-/-}$ yolk sacs showed reduced cell death as compared to *Hoil-1*$^{-/-}$ embryos (Fig. 1f, g). Although cell death was not completely ablated in *Tnfr1*$^{-/-}$*Hoil-1*$^{-/-}$ embryos, it did not appear to significantly affect yolk sac vasculature (Fig. 1f, g and Extended Data Fig. 2e). Nevertheless, *Tnfr1*$^{-/-}$*Hoil-1*$^{-/-}$ embryos died at around E16.5 (Extended Data Fig. 2d, f), with heart defects before death (Fig. 1h). Therefore, like HOIP, HOIL-1 is required to maintain blood vessel integrity by preventing TNFR1-mediated endothelial cell death during embryogenesis.

To understand the role of HOIL-1 in LUBAC function, we compared the formation of the TNFR1 signalling complex (TNFR1-SC) in mouse embryonic fibroblasts (MEFs) individually deficient for the LUBAC components. Although TNFR1-SC-associated linear ubiquitination was merely reduced in SHARPIN-deficient MEFs[7], it was completely absent in *Tnf*$^{-/-}$*Hoil-1*$^{-/-}$ MEFs, exactly as in *Tnf*$^{-/-}$*Hoip*$^{-/-}$ MEFs[8] (Fig. 2a). In TNF-stimulated *Tnf*$^{-/-}$*Hoil-1*$^{-/-}$ MEFs, NF-κB activation was attenuated (Extended Data Fig. 3a) and TNFR1 complex-II formation was enhanced (Fig. 2b), resulting in sensitization to TNF-induced apoptosis and necroptosis (Fig. 2c). Hence, HOIL-1 is as essential as HOIP for linear ubiquitination within the TNFR1-SC.

To determine whether the reduction in HOIP and SHARPIN protein levels in HOIL-1-deficient cells was responsible for the observed loss of linear ubiquitination (Fig. 2a), we reconstituted HOIL-1-deficient MEFs with HOIP, with HOIP plus SHARPIN, or, as a control, with HOIL-1. Reconstitution with HOIP, either alone or with SHARPIN, failed to restore LUBAC recruitment, linear ubiquitination at the TNFR1-SC, or optimal NF-κB activation. Furthermore, the reconstitution of HOIP and/or SHARPIN was unable to prevent TNF-induced complex-II formation and cell death, whereas the re-expression of HOIL-1 corrected all aforementioned defects (Fig. 2d–f and Extended Data Fig. 3b). In the absence of HOIL-1, HOIP was unable to bind to SHARPIN despite both being reconstituted to near endogenous levels (Extended Data Fig. 3c). Thus, HOIL-1 is required for LUBAC assembly and recruitment to the TNFR1-SC, identifying it as an essential component of LUBAC alongside HOIP.

To reveal how HOIL-1 enables LUBAC activity, we generated HOIL-1-deficient MEFs stably expressing full-length wild-type HOIL-1, the UBL domain of HOIL-1 only (HOIL-1-UBL), HOIL-1-ΔRBR, HOIL-1-ΔUBL, HOIL-1 with inactivating mutations T201A/R208A in the NZF domain (HOIL-1-NZFmut) or HOIL-1 with a point mutation in the catalytic cysteine of the RBR domain (HOIL-1-C458A) (Fig. 2g). Except for HOIL-1-ΔUBL, all mutant HOIL-1 proteins bound to HOIP and SHARPIN and stabilized their levels (Fig. 2h). Isolation of the native TNFR1-SC revealed that HOIL-1-ΔRBR and HOIL-1-C458A fully restored TNF-induced linear ubiquitination in HOIL-1-deficient cells, whereas HOIL-1-ΔUBL did not (Fig. 2i). HOIL-1-deficient cells

[1]UCL Cancer Institute, University College London, London, UK. [2]Laboratory of Adaptive Immunity, Institute of Molecular Genetics, Czech Academy of Sciences, Prague, Czech Republic. [3]University of Texas Health Science Center, San Antonio, TX, USA. [4]UCL Great Ormond Street Institute of Child Health, London, UK. [5]Institute of General Pathology, Università Cattolica del Sacro Cuore, Rome, Italy. [6]The Walter and Eliza Hall Institute of Medical Research, Parkville, Victoria, Australia. [7]Department of Medical Biology, The University of Melbourne, Melbourne, Victoria, Australia. [8]Pattern Recognition Receptor Discovery Performance Unit, Immuno-Inflammation Therapeutic Area, GlaxoSmithKline, Collegeville, PA, USA. [9]These authors contributed equally: Nieves Peltzer, Maurice Darding. *e-mail: h.walczak@ucl.ac.uk

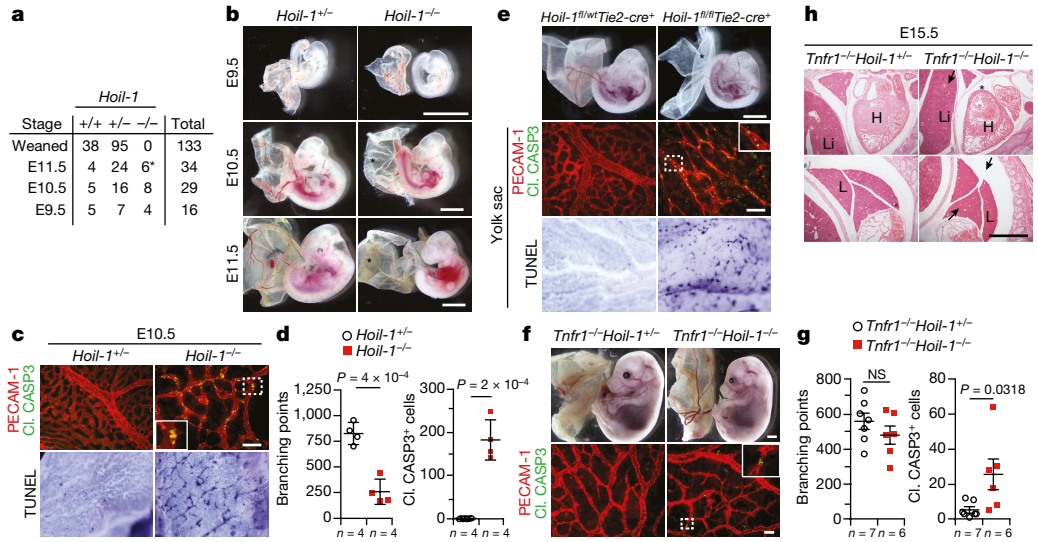

Fig. 1 | HOIL-1 deficiency causes embryonic lethality at mid-gestation due to TNFR1-mediated endothelial cell death. a, Mendelian frequencies obtained from inter-crossing *Hoil-1*$^{+/-}$ mice. Asterisk denotes dead embryos. **b**, Representative images of embryos from E9.5 to E11.5 quantified in **a**. Asterisks denote poor yolk sac vascularization. Scale bars, 2 mm. **c**, Top, representative images of yolk sac vascularization (PECAM-1, red) and cell death (cleaved (Cl.) CASP3 staining, green) at E10.5 ($n = 4$ yolk sacs per genotype). Bottom, whole-mount TUNEL staining ($n = 2$ yolk sacs per genotype). Scale bars, 50 μm. **d**, **g**, Quantification of branching points and cleaved CASP3-positive cells in **c** and **f**. Data are mean ± s.e.m. *P* values from unpaired two-tailed *t*-tests are shown. NS, not significant. **e**, Top, representative images of embryos at E10.5 ($n = 14$ *Hoil-1*$^{fl/wt}$*Tie2-cre*$^{+}$ and $n = 7$ *Hoil-1*$^{fl/fl}$*Tie2-cre*$^{+}$ embryos, top). Asterisk denotes poor yolk sac vascularization. Scale bar, 2 mm. Middle, yolk sac vascularization (PECAM-1, red) and apoptosis (cleaved CASP3, green). Scale bar, 50 μm. Bottom, yolk sac whole-mount TUNEL staining ($n = 6$ *Hoil-1*$^{fl/wt}$*Tie2-cre*$^{+}$ and $n = 2$ *Hoil-1*$^{fl/fl}$*Tie2-cre*$^{+}$ yolk sacs per genotype). **f**, Top, representative images of embryos at E15.5 ($n = 6$ *Tnfr1*$^{-/-}$*HOIL-1*$^{-/-}$ and $n = 19$ *Tnfr1*$^{-/-}$*Hoil-1*$^{+/-}$ embryos). Scale bar, 2 mm. Bottom, yolk sac vascularization (PECAM-1, red) and apoptosis (cleaved CASP3, green). Scale bar, 50 μm. **h**, Representative images of haematoxylin and eosin (H&E) staining on whole-embryo paraffin sections ($n = 3$ embryos per genotype). Asterisk denote pericardial effusion, arrows denote congested vessels. H, heart; L, lung; Li, liver. Scale bar, 50 μm.

expressing HOIL-1-UBL or HOIL-1-NZFmut only showed partial restoration of linear ubiquitination, correlating with reduced HOIP and SHARPIN levels at the TNFR1-SC (Fig. 2i). Thus, the UBL domain of HOIL-1 is essential for linear ubiquitination at the TNFR1-SC, whereas a functional NZF domain is required for optimal LUBAC presence in the TNFR1-SC. Expression of HOIL-1-ΔRBR restored optimal NF-κB signalling and prevented aberrant TNF-induced cell killing in contrast to HOIL-1-ΔUBL (Fig. 2j and Extended Data Fig. 3d). This observation explains why the previously reported mice, regarded as deficient for HOIL-1, are viable as they were generated by targeting exons 7 and 8[11], probably resembling the HOIL-1-ΔRBR mutant studied here. Because the UBL of HOIL-1 binds to HOIP, allowing its activation[12], and the NZF of HOIL-1 binds linear ubiquitin linkages[13] our results provide evidence that HOIL-1 promotes HOIP activation as well as LUBAC assembly and recruitment to the TNFR1-SC via its UBL domain. Once linear ubiquitin chains are formed in the complex, the NZF domain of HOIL-1 promotes LUBAC retention by binding to these chains.

Because both HOIL-1 and HOIP are equally important for LUBAC function and, consequently, for preventing aberrant cell death in vitro and in vivo, we used a genetic strategy to untangle the interaction between HOIL-1 or HOIP and the different cell death components. Inactivation of RIPK1 in *Hoil-1*$^{-/-}$ and *Hoip*$^{-/-}$ embryos delayed lethality until E14.5 (Fig. 3a and Extended Data Fig. 4a–d). At this time, *Ripk1*^{K45A}*Hoil-1*$^{-/-}$ and *Ripk1*^{K45A}*Hoip*$^{-/-}$ embryos had disrupted vascular architecture, excessive cell death in their yolk sacs, hearts, livers and lungs, and presented with heart defects and liver necrosis (Fig. 3b and Extended Data Fig. 4e–h). In accordance, TNFR1 complex-II formation and aberrant apoptosis induced by TNF or lymphotoxin-α (LT-α) were only partially inhibited in RIP1 kinase-dead *Ripk1*^{K45A}*Hoil-1*$^{-/-}$ MEFs (Fig. 3c, d and Extended Data Fig. 4i). Thus, although the kinase activity of RIPK1 is essential for excessive TNFR1-induced cell death caused by attenuated LUBAC activity, as previously observed in SHARPIN-deficient mice[4], this is not the case when LUBAC activity is completely abrogated.

We next tested whether the loss of RIPK3, MLKL or caspase-8 could prevent lethality in *Hoip*$^{-/-}$ and *Hoil-1*$^{-/-}$ embryos. At E10.5, *Ripk3*$^{-/-}$*Hoil-1*$^{-/-}$ embryos presented with defects in vascularization, excessive cell death and died at mid-gestation (Extended Data Fig. 5b, c). Owing to the close chromosomal linkage of HOIP and RIPK3, we generated *Mlkl*$^{-/-}$*Hoip*$^{-/-}$ mice (Extended Data Fig. 5a). These embryos also died at mid-gestation (Extended Data Fig. 5d). Likewise, neither *Casp8* heterozygosity nor full deletion was sufficient to prevent the mid-gestation lethality of *Hoip*$^{-/-}$ and *Hoil-1*$^{-/-}$ embryos (Extended Data Fig. 5e, f and data not shown).

As RIPK3-mediated necroptosis may be responsible for the embryonic lethality of *Casp8*$^{+/-}$*Hoil-1*$^{-/-}$ or *Casp8*$^{-/-}$*Hoil-1*$^{-/-}$ mice[14,15], we generated *Ripk3*$^{-/-}$*Casp8*$^{+/-}$*Hoil-1*$^{-/-}$ and *Ripk3*$^{-/-}$*Casp8*$^{-/-}$*Hoil-1*$^{-/-}$ embryos and in both cases the lethality was delayed until around E14.5 (Fig. 3e and Extended Data Fig. 6a, b). At this developmental stage, a single intact copy of caspase-8 was sufficient to induce apoptosis-driven loss of yolk sac vascularization (Fig. 3f and Extended Data Fig. 6c, d). Yet, although *Ripk3*$^{-/-}$*Casp8*$^{-/-}$*Hoil-1*$^{-/-}$ embryos died around E14.5, yolk sac vascularization was normalized and cell death in the yolk sac and other organs was prevented (Fig. 3f and Extended Data Fig. 6c–f). Moreover, *Ripk3*$^{-/-}$*Casp8*$^{-/-}$*Hoil-1*$^{-/-}$ MEFs were resistant to cell death induced by TNF or related cytokines (Extended Data Fig. 6g). Histological examination and microfocus computed tomography scanning revealed the presence of heart defects in both *Ripk3*$^{-/-}$*Casp8*$^{-/-}$*Hoil-1*$^{-/-}$ and *Ripk3*$^{-/-}$*Casp8*$^{+/-}$*Hoil-1*$^{-/-}$ embryos (Extended Data Fig. 6h, i). We therefore conclude that whereas mid-gestation lethality in *Hoil-1*$^{-/-}$ embryos is dependent on caspase-8/RIPK3-mediated apoptosis and necroptosis, *Ripk3*$^{-/-}$*Casp8*$^{-/-}$*Hoil-1*$^{-/-}$ embryos die at late gestation by a process that is independent of cell death.

In marked contrast to *Ripk3*$^{-/-}$*Casp8*$^{-/-}$*Hoil-1*$^{-/-}$ mice, both *Mlkl*$^{-/-}$*Casp8*$^{-/-}$*Hoil-1*$^{-/-}$ and *Mlkl*$^{-/-}$*Casp8*$^{-/-}$*Hoip*$^{-/-}$ mice were born, albeit at lower than expected Mendelian ratios (Fig. 3g and Extended Data Fig. 7a). These mice were runted and had to be

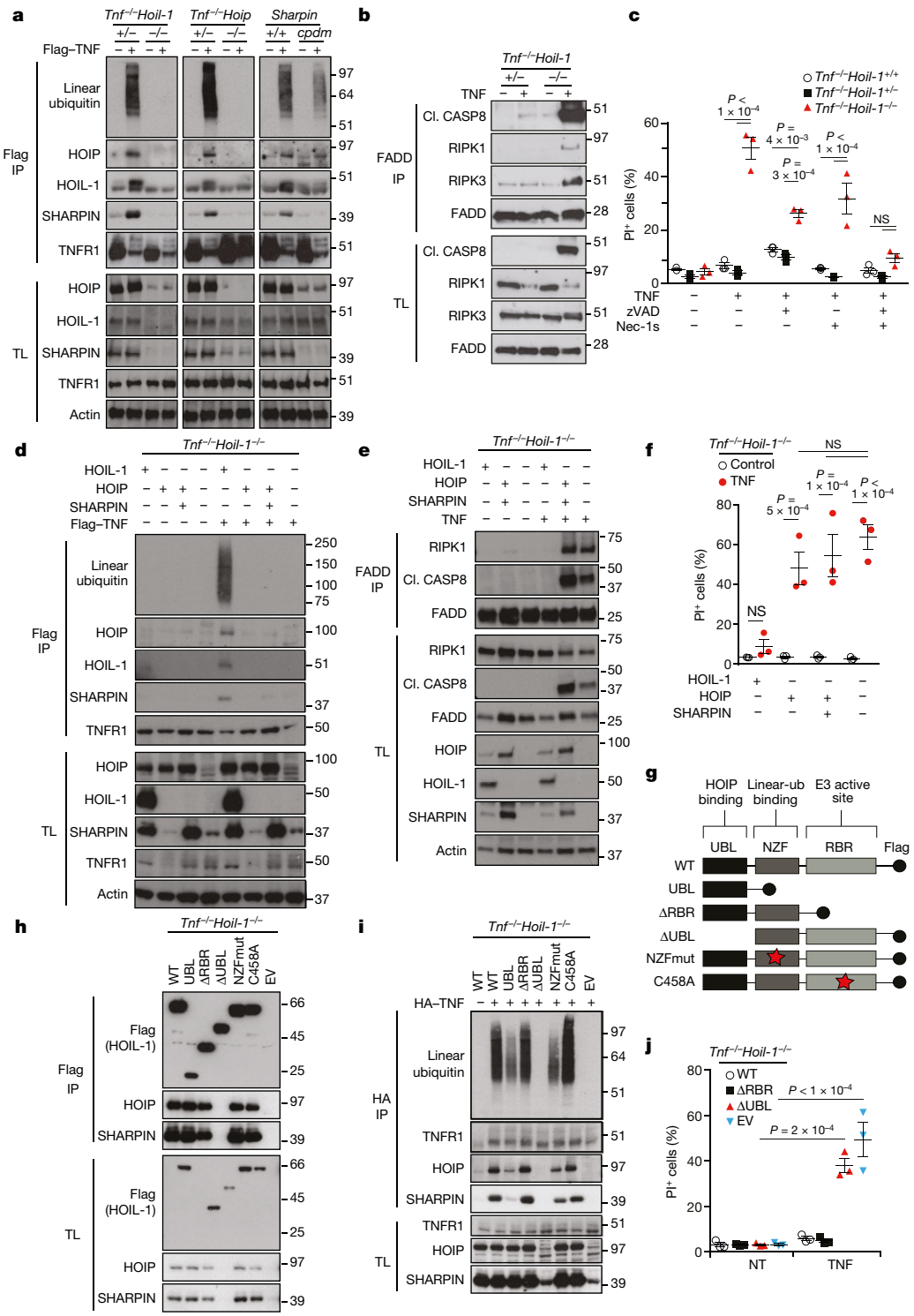

Fig. 2 | The UBL domain but not the RBR domain of HOIL-1 is essential for LUBAC activity at the TNFR1-SC and to prevent TNF/TNFR1-induced cell death. a, **d**, TNFR1-SC pull-down by Flag immunoprecipitation (IP) in MEFs derived from mice of the indicated genotypes ± Flag–TNF for 15 min ($n = 2$ independent experiments) (**a**) and reconstituted with HOIL-1, HOIP or HOIP and SHARPIN ($n = 4$ independent experiments) (**d**). **b**, **e**, Immunoprecipitation of the adaptor protein FADD in MEFs of the indicated genotypes treated for 4 h with the caspase inhibitor zVAD-fmk ± TNF (**b**) and reconstituted as indicated (**e**) ($n = 2$ independent experiments (**b**, **e**)). **c**, **f**, **j**, Cell death analysed by propidium iodide (PI) staining in MEFs with the indicated genotypes ± TNF ± the indicated inhibitors zVAD-fmk (zVAD) and/or necrostatin-1 (Nec-1s) for 24 h (**c**), reconstituted (**f**) or transduced (**j**) as indicated. Mean ± s.e.m. ($n = 3$ independent experiments) and P values from two-way ANOVA are shown. **g**, Schematic overview of HOIL-1 constructs used to transduce $Tnf^{-/-}Hoil\text{-}1^{-/-}$ MEFs. WT, wild type. **h**, Flag immunoprecipitation of indicated HOIL-1 mutants ($n = 2$ independent experiments). **i**, Endogenous TNFR1-SC pull-down by haemagglutinin (HA) immunoprecipitation in reconstituted $Tnf^{-/-}Hoil\text{-}1^{-/-}$ MEFs ± HA–TNF for 15 min ($n = 2$ independent experiments). EV, empty vector; NT, not treated; TL, total lysate. For gel source data (**a**, **b**, **d**, **e**, **h**, **i**), see Supplementary Fig. 1.

euthanized by 4–5 weeks of age (Fig. 3h, Extended Data Fig. 7b, c). Histopathological analysis revealed severe inflammation in the liver and lungs (Extended Data Fig. 7d and data not shown). Of note, *Casp8* heterozygosity resulted in increased apoptosis of endothelial cells, causing lethality in both $Mlkl^{-/-}Casp8^{+/-}Hoip^{-/-}$ and $Mlkl^{-/-}Casp8^{+/-}Hoil\text{-}1^{-/-}$ embryos around E14.5 (Extended Data

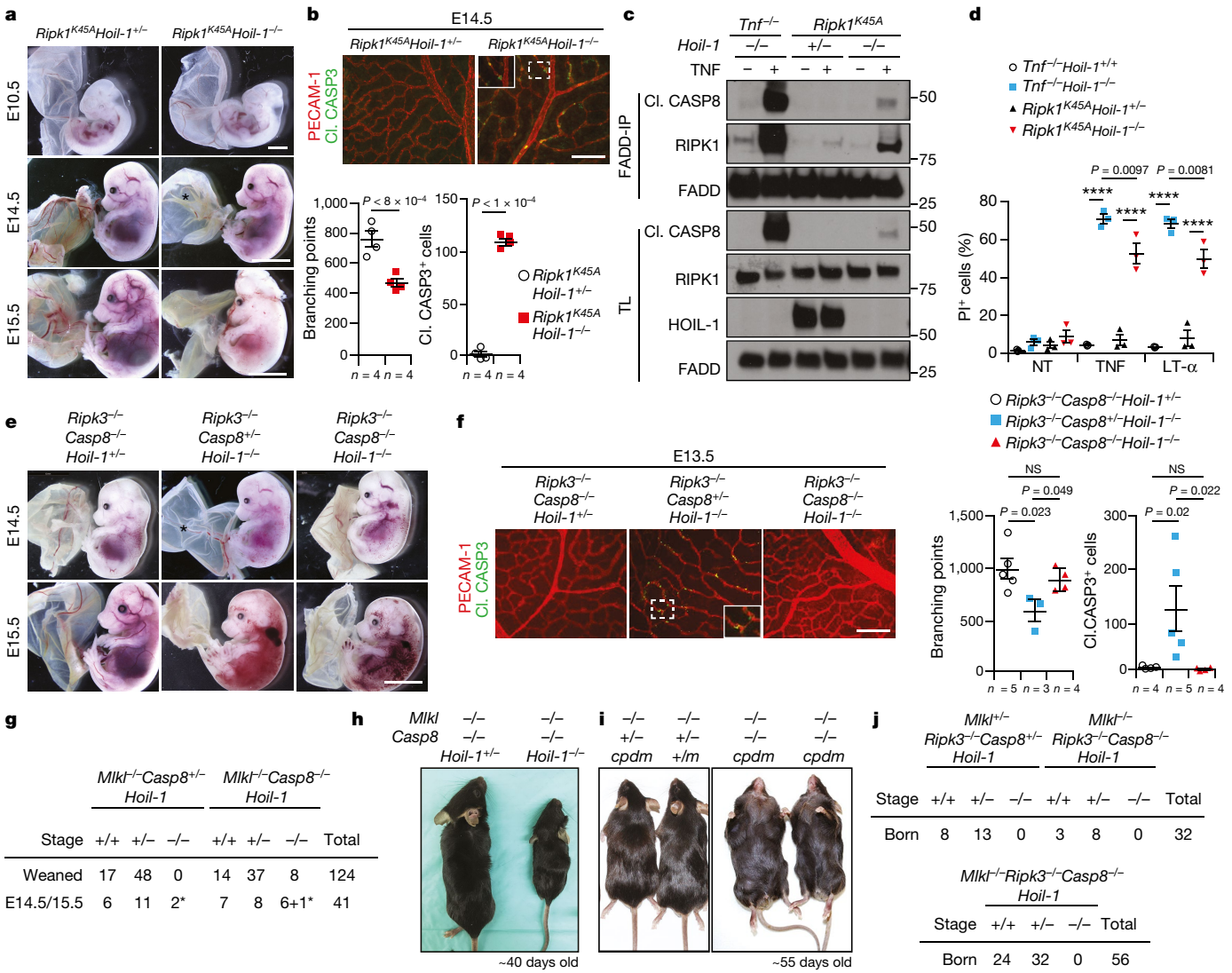

g

	Mlkl–/–Casp8+/– Hoil-1			Mlkl–/–Casp8–/– Hoil-1			
Stage	+/+	+/–	–/–	+/+	+/–	–/–	Total
Weaned	17	48	0	14	37	8	124
E14.5/15.5	6	11	2*	7	8	6+1*	41

h

i

j

	Mlkl+/– Ripk3–/–Casp8+/– Hoil-1			Mlkl–/– Ripk3–/–Casp8–/– Hoil-1			
Stage	+/+	+/–	–/–	+/+	+/–	–/–	Total
Born	8	13	0	3	8	0	32

	Mlkl–/–Ripk3–/–Casp8–/– Hoil-1			
Stage	+/+	+/–	–/–	Total
Born	24	32	0	56

Fig. 3 | Concomitant loss of MLKL and caspase-8, but not loss of RIPK1 kinase activity or combined loss of RIPK3 and caspase-8, promotes survival of LUBAC-deficient mice. a, Representative images of E10.5 ($n = 6$ embryos per genotype), E14.5 ($n = 12$ *Ripk1*^{K45A}*Hoil-1*$^{+/-}$, $n = 5$ *Ripk1*^{K45A}*Hoil-1*$^{-/-}$ embryos per genotype) and E15.5 embryos ($n = 3$ embryos per genotype). Scale bars, 2 mm (E10.5) and 5 mm (E14.5, E15.5). Asterisk denotes poor yolk sac vascularization. **b**, **f**, Representative images of yolk sac vascularization (PECAM-1, red) and apoptosis (cleaved (Cl.) CASP3, green) at E14.5 (**b**) or E13.5 (**f**) and quantification. Mean ± s.e.m. and *P* values from unpaired two-tailed *t*-tests (**b**) or one-way ANOVA (**f**) are shown. Scale bar, 50 μm. **c**, Immunoprecipitation of the adaptor protein FADD in MEFs treated for 3 h with TNF and zVAD-fmk ($n = 2$ independent experiments). For gel source data, see Supplementary Fig. 1. **d**, Cell death measured by propidium iodide (PI) incorporation in MEFs treated with TNF (10 ng ml^{-1}) or LT-α, or not treated (NT). Data are mean ± s.e.m. ($n = 3$ independent experiments). ****$P < 0.0001$, two-way ANOVA. **e**, Representative images of E14.5 ($n = 11$ *Ripk3*$^{-/-}$*Casp8*$^{-/-}$*Hoil-1*$^{+/-}$, *Ripk3*$^{-/-}$*Casp8*$^{+/-}$*Hoil-1*$^{-/-}$ and $n = 7$ *Ripk3*$^{-/-}$*Casp8*$^{-/-}$*Hoil-1*$^{-/-}$) and E15.5 ($n = 5$ *Ripk3*$^{-/-}$*Casp8*$^{-/-}$*Hoil-1*$^{+/-}$, $n = 4$ *Ripk3*$^{-/-}$*Casp8*$^{+/-}$*Hoil-1*$^{-/-}$ and $n = 8$ *Ripk3*$^{-/-}$*Casp8*$^{-/-}$*Hoil-1*$^{-/-}$) embryos. Asterisk denotes poor yolk sac vascularization. Scale bar, 5 mm. **g**, **j**, Mendelian frequencies obtained from intercrossing *Mlkl*$^{-/-}$*Casp8*$^{+/-}$*Hoil-1*$^{+/-}$ with *Mlkl*$^{-/-}$*Casp8*$^{-/-}$*Hoil-1*$^{+/-}$ mice (**g**) or *Mlkl*$^{+/-}$*Ripk3*$^{-/-}$*Casp8*$^{-/-}$*Hoil-1*$^{+/-}$ with *Mlkl*$^{-/-}$*Ripk3*$^{-/-}$*Casp8*$^{-/-}$*Hoil-1*$^{+/-}$ mice (**j**, top) or *Mlkl*$^{-/-}$*Ripk3*$^{-/-}$*Casp8*$^{-/-}$*Hoil-1*$^{+/-}$ mice (**j**, bottom). Asterisk denotes dead embryo. **h**, **i**, Representative images of adult mice quantified in **g** (**h**), or $n = 3$ mice per genotype in **i**. *m* denotes *cpdm* mutation.

Fig. 7e and data not shown) indicating that caspase-8-driven apoptosis is sufficient to cause embryonic death of LUBAC-deficient embryos.

Co-deletion of RIPK3 and caspase-8 causes embryonic lethality in otherwise viable SHARPIN-deficient *cpdm* (chronic proliferative dermatitis mice, also known as *Sharpin*^{cpdm}) mice[7]. However, *Mlkl*$^{-/-}$*Casp8*$^{-/-}$*Sharpin*^{cpdm} mice were viable and the inflammatory syndrome that characterizes *Sharpin*^{cpdm} mice was prevented (Fig. 3i and Extended Data Fig. 7f, g), while expectedly[16] developing lymphadenopathy and splenomegaly (Fig. 3i and Extended Data Fig. 7f). Thus, the combined loss of any of the three LUBAC components together with the loss of caspase-8 uncovers a vital functional difference between RIPK3 and MLKL.

We next evaluated whether the lethality of *Ripk3*$^{-/-}$*Casp8*$^{-/-}$*Hoil-1*$^{-/-}$ mice is due to aberrant (RIPK3-independent) MLKL activation. This was particularly pertinent because MLKL levels were increased in *Ripk3*$^{-/-}$*Casp8*$^{-/-}$*Hoil-1*$^{-/-}$ embryos and MLKL was aberrantly activated in some of them (Extended Data Fig. 7h). However, MLKL co-deficiency did not prevent the death of *Ripk3*$^{-/-}$*Casp8*$^{-/-}$*Hoil-1*$^{-/-}$ embryos (Fig. 3j). Thus, RIPK3 is required for the survival of embryos in the absence of LUBAC by regulating an MLKL-independent process.

To explore the nature of the pro-survival role of RIPK3, we performed RNA sequencing (RNA-seq) on E13.5 *Ripk3*$^{-/-}$*Casp8*$^{-/-}$*Hoil-1*$^{-/-}$, *Mlkl*$^{-/-}$*Casp8*$^{-/-}$*Hoil-1*$^{-/-}$ and control embryos (Extended Data Fig. 8a and Supplementary Table 1). Gene Ontology (GO) enrichment analysis of differentially expressed genes pointed towards defects in erythropoiesis in *Ripk3*$^{-/-}$*Casp8*$^{-/-}$*Hoil-1*$^{-/-}$ embryos (Extended Data Fig. 8b). Indeed, reduced levels of erythroid lineage TER119^{+} cells

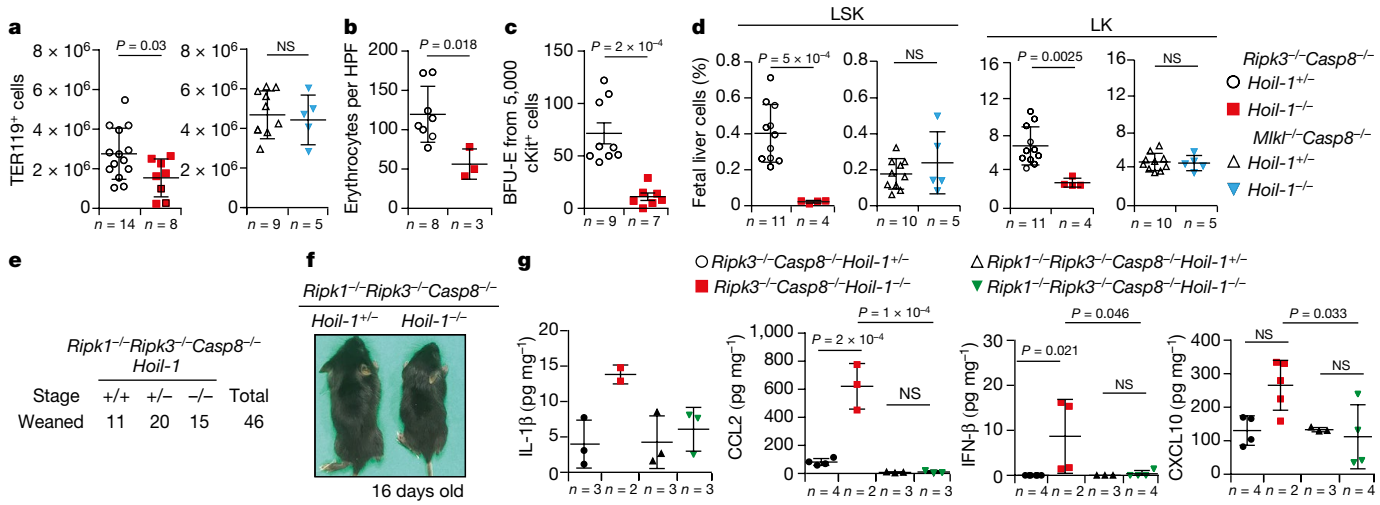

Fig. 4 | Combined deletion of RIPK3 and caspase-8 causes haematopoietic defects and RIPK1-dependent embryonic lethality in HOIL-1-deficient mice. a, **b**, Number of TER119$^+$ (erythroid) cells (**a**) and enucleated erythrocytes per high-power field (HPF) (**b**) in E13.5 fetal livers with the indicated genotypes. Data are mean ± s.e.m. *P* values from unpaired two-tailed *t*-tests are shown. **c**, Differentiation of E13.5 fetal liver (c-KIT$^+$) progenitors into erythroid burst-forming units (BFU-E). Data are mean ± s.e.m. *P* values from unpaired two-tailed *t*-tests are reported. **d**, Percentage of haematopoietic progenitors negative for mature lineage markers (Lin$^-$) and SCA-1$^+$c-KIT$^+$ (LSK) and SCA-1$^-$c-KIT$^+$ (LK) in E13.5 fetal livers with the indicated genotypes. Data are mean ± s.e.m. *P* values from unpaired two-tailed *t*-tests are reported. **e**, Mendelian frequencies obtained from intercrossing *Ripk1*$^{-/-}$*Ripk3*$^{-/-}$*Casp8*$^{-/-}$*Hoil-1*$^{+/-}$ mice. **f**, Representative images of mice of the indicated genotypes quantified in **e**. **g**, Cytokine levels in embryo homogenates with the indicated genotypes. Data are mean ± s.e.m. *P* values from one-way ANOVA are reported.

(Fig. 4a), basophilic erythroblasts (Extended Data Fig. 8c) and mature erythrocytes (Fig. 4b) were observed in of *Ripk3*$^{-/-}$*Casp8*$^{-/-}$*Hoil-1*$^{-/-}$ fetal livers. Furthermore, *Ripk3*$^{-/-}$*Casp8*$^{-/-}$*Hoil-1*$^{-/-}$ haematopoietic progenitors failed to differentiate into committed erythroid burst-forming units (BFU-E) in culture (Fig. 4c). Further analysis of the haematopoietic compartment from E13.5 fetal livers revealed abnormally reduced percentages and total numbers of multipotent progenitors (Fig. 4d and Extended Data Fig. 8d, e) as well as leucocytes, including granulocytes and macrophages, and myeloid progenitors in the *Ripk3*$^{-/-}$*Casp8*$^{-/-}$*Hoil-1*$^{-/-}$ embryos compared to controls, whereas *Mlkl*$^{-/-}$*Casp8*$^{-/-}$*Hoil-1*$^{-/-}$ embryos had normal numbers of these cells (Extended Data Fig. 8f–k). In addition, the capacity of haematopoietic progenitors to generate colony-forming myeloid progenitors and multipotent progenitors was also impaired in the *Ripk3*$^{-/-}$*Casp8*$^{-/-}$*Hoil-1*$^{-/-}$ embryos (Extended Data Fig. 8l). Accordingly, the viability of macrophages obtained from *Ripk3*$^{-/-}$*Casp8*$^{-/-}$*Hoil-1*$^{-/-}$ fetal liver cell suspensions in culture was significantly lower than those of controls and this could not be rescued by inhibiting necroptosis or apoptosis. *Mlkl*$^{-/-}$*Casp8*$^{-/-}$*Hoil-1*$^{-/-}$ fetal liver cells, however, produced normal numbers of macrophages (Extended Data Fig. 4m). Despite the heart defects of *Ripk3*$^{-/-}$*Casp8*$^{-/-}$*Hoil-1*$^{-/-}$ embryos, blood circulation was normal at E13.5 and the percentages of CD45$^+$cKIT$^+$ cells obtained from aorta–gonad–mesonephros (AGM) regions were comparable between *Ripk3*$^{-/-}$*Casp8*$^{-/-}$*Hoil-1*$^{-/-}$ embryos and controls at E11.5 (Extended Data Fig. 8o, p). We therefore conclude that *Ripk3*$^{-/-}$*Casp8*$^{-/-}$*Hoil-1*$^{-/-}$ embryos have defective early haematopoiesis, probably downstream of specification in the AGM, resulting in substantial deficiencies in erythroid and myeloid cells.

Because LUBAC is known to regulate RIPK1[17,18], we investigated the role of RIPK1 in the lethality of *Ripk3*$^{-/-}$*Casp8*$^{-/-}$*Hoil-1*$^{-/-}$ embryos. The lethality of *Ripk3*$^{-/-}$*Casp8*$^{-/-}$*Hoil-1*$^{-/-}$ embryos was prevented by additional loss of RIPK1, despite RIPK1 levels being relatively low in *Ripk3*$^{-/-}$*Casp8*$^{-/-}$*Hoil-1*$^{-/-}$ embryos and RIPK1 deficiency failing to prevent *Hoil-1*$^{-/-}$ embryonic lethality (Fig. 4d, e and Extended Data Figs. 7h, 9a, b). Importantly, the viability of macrophages obtained from *Ripk1*$^{-/-}$*Ripk3*$^{-/-}$*Casp8*$^{-/-}$*Hoil-1*$^{-/-}$ fetal livers was comparable to controls (Extended Data Fig. 9c), indicating normalized haematopoiesis in these mice. The expression of several cytokines, including IL-1β, CCL2, IFN-β and CXCL10, was abnormally increased in *Ripk3*$^{-/-}$*Casp8*$^{-/-}$*Hoil-1*$^{-/-}$ embryos but not in *Ripk1*$^{-/-}$*Ripk3*$^{-/-}$*Casp8*$^{-/-}$*Hoil-1*$^{-/-}$ embryos (Fig. 4f and Extended Data Fig. 9d, e). The function, survival, differentiation and self-renewal of haematopoietic progenitors are greatly impacted by several of these cytokines[19,20]. Therefore, our findings suggest that RIPK1-driven deregulated cytokine production in *Ripk3*$^{-/-}$*Casp8*$^{-/-}$*Hoil-1*$^{-/-}$ embryos may impair fetal haematopoiesis. Finally, the treatment of pregnant females with the RIPK1 kinase inhibitor GSK3540547A (GSK'547A)[21] did not prevent lethality of *Ripk3*$^{-/-}$*Casp8*$^{-/-}$*Hoil-1*$^{-/-}$ embryos, although it was able to extend the survival of *Ripk3*$^{-/-}$*Casp8*$^{+/-}$*Hoil-1*$^{-/-}$ embryos (Extended Data Fig. 9f). These results suggest that the lethality of *Ripk3*$^{-/-}$*Casp8*$^{-/-}$*Hoil-1*$^{-/-}$ embryos probably depends on the scaffolding function of RIPK1.

Although RIPK1 is required for emergency haematopoiesis, RIPK1 might regulate embryonic haematopoiesis differently. Indeed, RIPK1-constitutive or RIPK1-haematopoietic-cell-specific-deficient mice are not embryonically lethal[22,23]. In addition, the absence of LUBAC, RIPK3 and caspase-8 might affect mechanisms during embryogenesis that are different from those perturbed by RIPK1 deficiency alone. Collectively, our findings indicate that in the combined absence of LUBAC and caspase-8, RIPK3 exerts a pro-survival role by regulating RIPK1-mediated signalling (Extended Data Fig. 10). Because *Ripk3*$^{-/-}$*Casp8*$^{-/-}$ mice are viable[14,15,24], our findings indicate that the control of RIPK1 by either LUBAC or RIPK3 is sufficient to enable proper haematopoiesis in the developing embryo, probably by preventing deregulated cytokine production. Thus, LUBAC and RIPK3 control RIPK1-mediated signalling to allow embryonic haematopoiesis.

Online content

Any Methods, including any statements of data availability and Nature Research reporting summaries, along with any additional references and Source Data files, are available in the online version of the paper at https://doi.org/10.1038/s41586-018-0064-8.

Received: 21 October 2016; Accepted: 16 March 2018;
Published online 25 April 2018.

1. Shimizu, Y., Taraborrelli, L. & Walczak, H. Linear ubiquitination in immunity. *Immunol. Rev.* **266**, 190–207 (2015).

2. Sasaki, Y. et al. Defective immune responses in mice lacking LUBAC-mediated linear ubiquitination in B cells. *EMBO J* **32**, 2463–2476 (2013).
3. Emmerich, C. H. et al. Activation of the canonical IKK complex by K63/M1-linked hybrid ubiquitin chains. *Proc. Natl Acad. Sci. USA* **110**, 15247–15252 (2013).
4. Berger, S. B. et al. Cutting edge: RIP1 kinase activity is dispensable for normal development but is a key regulator of inflammation in SHARPIN-deficient mice. *J. Immunol.* **192**, 5476–5480 (2014).
5. Gerlach, B. et al. Linear ubiquitination prevents inflammation and regulates immune signalling. *Nature* **471**, 591–596 (2011).
6. Kumari, S. et al. Sharpin prevents skin inflammation by inhibiting TNFR1-induced keratinocyte apoptosis. *eLife* **3**, e03422 (2014).
7. Rickard, J. A. et al. TNFR1-dependent cell death drives inflammation in *Sharpin*-deficient mice. *eLife* **3**, e03464 (2014).
8. Peltzer, N. et al. HOIP deficiency causes embryonic lethality by aberrant TNFR1-mediated endothelial cell death. *Cell Reports* **9**, 153–165 (2014).
9. Boisson, B. et al. Immunodeficiency, autoinflammation and amylopectinosis in humans with inherited HOIL-1 and LUBAC deficiency. *Nat. Immunol* **13**, 1178–1186 (2012).
10. Boisson, B. et al. Human HOIP and LUBAC deficiency underlies autoinflammation, immunodeficiency, amylopectinosis, and lymphangiectasia. *J. Exp. Med.* **212**, 939–951 (2015).
11. Tokunaga, F. et al. Involvement of linear polyubiquitylation of NEMO in NF-κB activation. *Nat. Cell Biol.* **11**, 123–132 (2009).
12. Stieglitz, B., Morris-Davies, A. C., Koliopoulos, M. G., Christodoulou, E. & Rittinger, K. LUBAC synthesizes linear ubiquitin chains via a thioester intermediate. *EMBO Rep.* **13**, 840–846 (2012).
13. Sato, Y. et al. Specific recognition of linear ubiquitin chains by the Npl4 zinc finger (NZF) domain of the HOIL-1L subunit of the linear ubiquitin chain assembly complex. *Proc. Natl Acad. Sci. USA* **108**, 20520–20525 (2011).
14. Kaiser, W. J. et al. RIP3 mediates the embryonic lethality of caspase-8-deficient mice. *Nature* **471**, 368–372 (2011).
15. Oberst, A. et al. Catalytic activity of the caspase-8-FLIP$_L$ complex inhibits RIPK3-dependent necrosis. *Nature* **471**, 363–367 (2011).
16. Alvarez-Diaz, S. et al. The pseudokinase MLKL and the kinase RIPK3 have distinct roles in autoimmune disease caused by loss of death-receptor-induced apoptosis. *Immunity* **45**, 513-526 (2016).
17. Peltzer, N., Darding, M. & Walczak, H. Holding RIPK1 on the ubiquitin leash in TNFR1 signaling. *Trends Cell Biol.* **26**, 445–461 (2016).
18. Annibaldi, A. & Meier, P. Checkpoints in TNF-induced cell death: implications in inflammation and cancer. *Trends Mol Med.* **24**, 49–65 (2018).
19. Clapes, T., Lefkopoulos, S. & Trompouki, E. Stress and non-stress roles of inflammatory signals during HSC emergence and maintenance. *Front. Immunol.* **7**, 487 (2016).
20. Pietras, E. M. Inflammation: a key regulator of hematopoietic stem cell fate in health and disease. *Blood* **130**, 1693–1698 (2017).
21. Harris, P. A. et al. Discovery of a first-in-class receptor interacting protein 1 (RIP1) kinase specific clinical candidate (GSK2982772) for the treatment of inflammatory diseases. *J. Med. Chem.* **60**, 1247–1261 (2017).
22. Roderick, J. E. et al. Hematopoietic RIPK1 deficiency results in bone marrow failure caused by apoptosis and RIPK3-mediated necroptosis. *Proc. Natl Acad. Sci. USA* **111**, 14436–14441 (2014).
23. Rickard, J. A. et al. RIPK1 regulates RIPK3-MLKL-driven systemic inflammation and emergency hematopoiesis. *Cell* **157**, 1175–1188 (2014).
24. Dillon, C. P. et al. Survival function of the FADD-CASPASE-8-cFLIP$_L$ complex. *Cell Reports* **1**, 401–407 (2012).

Acknowledgements V. Dixit and K. Newton provided *Ripk3*$^{-/-}$ mice, S. Hedrick and R. Hakem provided *Casp8*$^{fl/fl}$ mice; H. Anderton and U. Nachbur helped with *Sharpin*^{cpdm} analysis; P. Levy and staff and L. Lawrence provided technical and histology services. A. Leister and J. Marinis advised on GSK'457A. T. Marafioti and A. Akarsa helped with phosphorylated MLKL detection. A. Annibaldi provided scientific advice and helpful discussions. B. J. Ferguson provided reagents and advice. The flow cytometry, microscopy and imaging core facilities are supported by Cancer Research UK through the CRUK-UCL Centre (515818) and a Cancer Immunotherapy Accelerator award (CITA, 525877). This work was funded by a Wellcome Trust Senior Investigator Award (096831/Z/11/Z), an ERC Advanced grant (294880) and a Cancer Research UK programme grant (A17341) awarded to H.W., NHMRC grants awarded to P.B., A. St., J.S. and H.W. (602516, 1037321, 1043414, 1080321, 1105209, 461221, 1042629, 1057905), the Leukemia and Lymphoma Society (Specialised Center of Research grant 7015) and a postdoctoral fellowship awarded to N.P. by the Swiss National Science Foundation (P300P3_158509).

Reviewer information *Nature* thanks F. Chan and the other anonymous reviewer(s) for their contribution to the peer review of this work.

Author contributions H.W. conceived the project. N.P. and M.D. performed most experiments. N.P., M.D. and H.W. designed the research and co-wrote the manuscript. A.M., C.B. and T.E. conceived and contributed to the haematopoietic analyses. H.D. and P.D. contributed to in vitro experiments in Fig. 2 and Extended Data Fig. 3, S.K. generated *Mlkl*$^{-/-}$ mice, L.T., E.R. contributed to in vivo experiments, T.H performed cytokine arrays and E.L. and Y.S. contributed with biochemistry data. P.B., T.L.H. and H.W. designed the *Hoil-1*-floxed allele and P.B. generated it. A.F. and W.K. generated and analysed *Ripk1*$^{-/-}$*Ripk3*$^{-/-}$*Casp8*$^{-/-}$*Hoil-1*$^{-/-}$ mice. H.D. and A.Sa. performed genotyping. A.B. and J.B. provided GSK'547A and *Ripk1*^{K45A} mice. J.R., S.A.-D., A.St. and J.S. performed the *Sharpin*^{cdpm} studies. C.H. and M.T.A. performed pathological and microfocus computed tomography analyses. T.E., P.B., A.St., J.S. and E.R. provided scientific insight.

Competing interests J.B and A.L. are GSK employees.

Additional information
Extended data is available for this paper at https://doi.org/10.1038/s41586-018-0064-8.
Supplementary information is available for this paper at https://doi.org/10.1038/s41586-018-0064-8.
Reprints and permissions information is available at http://www.nature.com/reprints.
Correspondence and requests for materials should be addressed to H.W.
Publisher's note: Springer Nature remains neutral with regard to jurisdictional claims in published maps and institutional affiliations.

METHODS

Mice. The *Hoil-1*-floxed (*Hoil-1*$^{fl/fl}$) mice were generated by a gene-targeting strategy in ES cells in which the targeting cassette was composed of a hygromycin-resistance cassette flanked by *Frt* sites and exons 1 and 2 of the *Hoil-1* gene flanked by *loxP* sites. Southern blots of C57BL/6 ES cell clones containing the homologous recombination were analysed for the specificity of the recombination and the absence of any unwanted integration. Two ES cell clones were used to generate mutant animals on the C57BL/6 genetic background, corresponding to the two independent *Hoil-1*$^{-/-}$ strains (*Hoil-1*$^{-/-}$ and C20*Hoil-1*$^{-/-}$). The hygromycin cassette was removed by crossing these mice with C57BL/6 mice expressing the FlpE recombinase and this was followed by a cross with C57BL/6 mice to remove the flpe transgene. *Hoip*$^{-/-}$ and *Hoil-1*$^{-/-}$ mice were generated by crossing *Hoip*$^{fl/fl}$ mice, previously described[17], and *Hoil-1*$^{fl/fl}$ mice (described here) with transgenic mice expressing the *loxP*-deleter Cre recombinase (purchased from JAX: 6054, B6.C-Tg(CMV-Cre)1 Cgn/J). Transgenic mice expressing the Cre recombinase under the control of the *Tie2* (also known as *Tek*) promoter (*Tie2*-Cre) (B6.Cg-Tg(Tek-cre)1Ywa/J)[25] were used to delete floxed genes specifically in endothelial cells. C57BL/6 *Mlkl*$^{-/-}$ mice crossed to *Sharpin*^{cpdm} mice were previously described[26]. For all other crosses *Mlkl*$^{-/-}$ mice were generated using transcription activator-like effector nuclease (TALEN). In brief, TALENs targeting exon 1 of the *Mlkl* gene were cloned via Golden-gate assembly. The RVD sequence of TAL1 against TACCGTTTCAGATGTCA was NIHDHDNNNGNGNGHDNINNNINGNNNGHDNI, and TAL2 against TCGATCTTCCTGCTGCC was HDNNNINGHDNGNGHDHDNGNNHDNGN NHDHD. Capped RNA was produced in vitro using mMESSAGE mMACHINE T7 Transcription Kit (Ambion) and poly A tail was added using Poly(A) Tailing Kit (Ambion). Purified transcripts were mixed and adjusted to 25 ng μl^{-1}. C57BL/6 fertilized eggs were injected into both the cytoplasm and the pro-nucleus. Embryos were transferred into C57BL/6 pseudo-pregnant females. Pups were genotyped by sequencing using genomic DNA obtained from ear punches. One female carrying a 19-base pair (bp) homozygous deletion causing a premature stop codon was selected for further breeding. *Mlkl*$^{-/-}$ mice were backcrossed to C57BL/6 mice for two generations. *Sharpin*^{cpdm} (C57BL/Ka) and *Tnfr1*$^{-/-}$ (2818, B6.129-Tnfrsf1atm1Mak/J) mice were purchased from JAX. *Tnf*$^{-/-}$ mice (C57BL/6;129S6) were provided by W. Kaiser. *Ripk3*$^{-/-}$[27], *Casp8*$^{-/-}$[28], *Ripk1*^{K45A4} and *Ripk1*$^{-/-}$[29] mice have been reported previously. Timed matings were performed as previously described[8]. All mice were genotyped by PCR, fed ad libitum. All animal experiments were conducted under an appropriate UK project license in accordance with the regulations of UK home office for animal welfare according to ASPA (animal (scientific procedure) Act 1986). The relevant Animal Ethics Committee approved all experiments involving *Sharpin*^{cpdm} and the *Ripk1*$^{-/-}$ crosses which were maintained under appropriate licenses and subject to ethical review at The Walter and Eliza Hall Institute (Melbourne, Australia) and UT Health Sciences Center San Antonio (TX, USA), respectively.

Histological analysis, TUNEL and immunofluorescence staining. Embryos or organs from adult mice were collected and fixed in 10% buffered formalin and paraffin embedded. Sections of 4-μm were stained with haematoxylin and eosin following standard procedures. Necropsy of adult mice or six sagittal serial sections of two different planes of the embryo were used for blinded pathological analysis. For TUNEL staining, sections were treated according to the manufacturer's instructions (DeadEnd Fluorometric TUNEL System, Promega, G3250). For whole-mount TUNEL staining and immunofluorescence staining, samples were processed using the ApoTag plus Peroxidase In situ Apoptosis Detection Kit (Millipore, S7101) according to the manufacturer's instructions and as previously described[8]. Quantification was performed by an experimenter blinded to the genotype of the mice by using ImageJ Software on monochrome images of the whole yolk sac by measuring the area of positive staining. Alternatively, TUNEL-positive cells were counted on five different fields (10× magnification). Yolk sacs were stained with antibodies against PECAM-1 (BD Biosciences, 5533370 clone MEC13.3) and cleaved caspase 3 (Cell Signaling, 9664), followed by staining with secondary antibodies, Alexa Fluor 594 goat anti-rat IgG and Alexa Fluor 488 goat anti-rabbit IgG (Invitrogen, A-11007 and A-11034, respectively), and analysed by fluorescent microscopy. Quantification was performed by an experimenter blinded to the genotype of the mice on ten different fields (10× magnification) per yolk sac.

Microfocus computed tomography scan. Embryos were fixed in 4% paraformaldehyde and potassium triiodide (Lugol's iodine/I2KI, to impart tissue contrast), with a total iodine content of 63.25 mg ml^{-1} (iodine mass of 2.49 × 10^{-4} mol ml^{-1}), in a 1:1 ratio for 8 h before imaging. Before scanning, the embryos were washed, wrapped in Parafilm M (Bemis) and secured in 3% (w/v) Agar (Sigma-Aldrich), within a low-density plastic cylinder to ensure mechanical stability during scan acquisition. Images were acquired using an XT H 225 ST microfocus-computed tomography scanner with a multimetal target (Nikon Metrology). Scans were reconstructed using modified Feldkamp filtered back projection algorithms with proprietary software (CTPro3D; Nikon Metrology) and post-processed using VG Studio MAX (Volume Graphics GmbH). Soft tissues were analysed by Phong shading of direct volume renderings and plain projections and the vascular system by maximum intensity projections.

Cells. MEFs were isolated from E12.5–E13.5 embryos in accordance with standard procedures and these cells were maintained in DMEM medium supplemented with 10% fetal bovine serum (Sigma). Transformation was performed by lentiviral infection with the SV40 large T antigen. For reconstitution experiments, the coding sequence of mouse HOIP, SHARPIN or HOIL-1 wild-type (WT), the UBL domain of HOIL-1 only (HOIL-1-UBL; amino acids 1–139), HOIL-1-ΔRBR (amino acids 1–252), HOIL-1-ΔUBL (amino acids 140–508), HOIL-1 with inactivating mutations T201A/R208A in the NZF domain (HOIL-1-NZFmut) or HOIL-1 with a point mutation in the catalytic cysteine of the RBR domain (HOIL-1-C458A) was inserted in MSCV vector followed by the internal ribosome entry site (IRES)-GFP sequence. These vectors were retrovirally transduced into MEFs and GFP-positive cells were sorted in a MoFlo cytometer (Beckman Coulter).

Immunoprecipitation. For isolation of the TNFR1-SC, transformed MEFs were stimulated with 3×Flag-2×Strep–TNF at 0.5 μg ml^{-1} for 15 min, and controls were left untreated. Cells were subsequently solubilised in lysis buffer (30 mM Tris-HCl (pH 7.4), 150 mM NaCl, 2 mM EDTA, 2 mM KCl, 10% glycerol, 1% Triton X-100, EDTA-free proteinase inhibitor cocktail (Roche, 5056489001) and 1× phosphatase-inhibitor cocktail 2 (Sigma, P5726-1ML)) at 4 °C for 30 min. The lysates were cleared by centrifugation, and 3×Flag-2×Strep–TNF (0.5 μg ml^{-1} per sample) was added to the untreated samples. Subsequently, the lysates were subjected to anti-Flag immunoprecipitation using M2 antibody coupled sepharose beads (Sigma, A2220-5ML) for 16 h. For immunoprecipitation of FADD, transformed MEFs were treated with 20 μM zVAD-fmk (Abcam, ab120487) in the presence or absence of 100 ng ml^{-1} 6×His–TNF for 3 h. Cells were lysed as described above and FADD was immunoprecipitated using anti-FADD antibody (Santa Cruz, sc-5559) and protein G Sepharose Beads (GE healthcare, 17-0618-01) at 4 °C for 4 h. For SHARPIN immunoprecipitation, anti-SHARPIN antibody (ProteinTech, 14626-1-AP) was used. For all immunoprecipitations, the beads were washed three times with lysis buffer. Proteins were eluted in 50 μl of LDS buffer (NuPAGE, Invitrogen) containing 50 mM dithiothreitol (DTT). Samples were analysed by western blotting.

Western blot analysis and antibodies. Whole embryos were snap-frozen and homogenized in RIPA buffer (50 mM Tris pH 8.0, 150 mM NaCl, 0.5% sodium deoxycholate, 1% NP-40 and 1× EDTA-free proteinase inhibitor cocktail (Roche, 5056489001) or RIPA buffer with 6 M urea for the experiment in Extended data Fig. 7h. Alternatively, cells were washed twice with ice-cold PBS before lysis in lysis buffer. Protein concentration of lysates was determined using BCA protein assay (Thermo Scientific). Lysates were subsequently denatured in reducing sample buffer at 95 °C for 10 min before separation by SDS–PAGE (NuPAGE) and subsequent analysis by western blotting using antibodies against HOIL-1[30], HOIP (custom-made, Thermo Fisher Scientific), SHARPIN (ProteinTech, 14626-1-AP), TNFR1 (Abcam, ab19139), actin (Sigma, A1978), pIκBα (Cell Signaling, 9246), IκBα (Cell Signaling, 9242), phospho p65 (Cell Signaling, 3033) cleaved caspase-8 (Cell Signaling, 9429), linear ubiquitin (Merck Millipore, MABS199), RIPK1 (BD, 610459), RIPK3 (Enzo, ADI-905-242-100), FADD (Assay Design, AAM-121), MLKL (Millipore, MABC604), phospho-MLKL (Abcam, ab196436) and tubulin (Sigma, T9026).

Cell death analysis by propidium iodide staining. Cells were seeded to 80% confluence and were then incubated with 100 ng ml^{-1} His-tagged TNF, 1 μg ml^{-1} CD95L-Fc, 1 μg ml^{-1} isoleucine zipper tagged murine TRAIL (iz-mTRAIL), 100 μg ml^{-1} poly(I:C) HMW (InvivoGen, tlrl-pic), 20 ng ml^{-1} IFN-γ (Peprotech, 315-05) or 100 ng ml^{-1} LT-α (Thermo Fisher Scientific, 10270-HNAE) for 24 h, unless otherwise indicated. When indicated the following inhibitors were used: 20 μM zVAD-FMK (Abcam, ab120487), 10 μM necrostatin-1 (Biovision, 2263-5). Supernatants and adherent cells were collected and resuspended in PBS containing 5 μg ml^{-1} propidium iodide. Propidium iodide-positive cells were enumerated by FACS (BD Accuri).

RNA-sequencing analysis. E13.5 embryos were snap frozen and RNA was prepared using the RNeasy minikit (Qiagen, 74104) according to the manufacturer's instruction. To generate the library, samples were processed using the KAPA mRNA HyperPrep Kit (KK8580) according to the manufacturer's instructions. In brief, mRNA was isolated from total RNA using Oligo dT beads to pull down poly-adenylated transcripts. The purified mRNA was fragmented using chemical fragmentation (heat and divalent metal cation) and primed with random hexamers. Strand-specific first strand cDNA was generated using reverse transcriptase in the presence of actinomycin D. The second cDNA strand was synthesized using dUTP in place of dTTP, to mark the second strand. The resultant cDNA was then 'A-tailed' at the 3′ end to prevent self-ligation and adaptor dimerization. Truncated adaptors, containing a T overhang were ligated to the A-tailed cDNA. Successfully ligated cDNA molecules were then enriched with limited cycle PCR. Libraries to be multiplexed in the same run were pooled in equimolar quantities, calculated from Qubit

and Bioanalyser fragment analysis. Samples were sequenced on the NextSeq 500 instrument (Illumina) using a 43-bp paired-end run. Run data were de-multiplexed and converted to fastq files using the Illumina bcl2fastq Conversion Software v2.18 on BaseSpace. Fastq files were then aligned to a reference genome using STAR on the BaseSpace RNA-Seq alignment app v1.1.0. Reads per transcript were counted using HTSeq and differential expression was estimated using the BioConductor package DESeq2 (BaseSpace app v1.0.0). Next, four groups of differentially regulated genes were analysed: low and high abundance *Ripk3*$^{-/-}$*Casp8*$^{-/-}$*Hoil-1*$^{+/-}$ versus *Mlkl*$^{-/-}$*Casp8*$^{-/-}$*Hoil-1*$^{+/-}$ embryos and low and high abundance in *Ripk3*$^{-/-}$*Casp8*$^{-/-}$*Hoil-1*$^{-/-}$ versus *Mlkl*$^{-/-}$*Casp8*$^{-/-}$*Hoil-1*$^{-/-}$ embryos. To identify genes that were specifically altered in the absence of HOIL-1, the Venny 2.1 software was used to exclude genes that were differentially expressed between *Ripk3*$^{-/-}$*Casp8*$^{-/-}$*Hoil-1*$^{+/-}$ and *Mlkl*$^{-/-}$*Casp8*$^{-/-}$*Hoil-1*$^{+/-}$ embryos from those between *Ripk3*$^{-/-}$*Casp8*$^{-/-}$*Hoil-1*$^{-/-}$ and *Mlkl*$^{-/-}$*Casp8*$^{-/-}$*Hoil-1*$^{-/-}$ embryos. Genes that were already differentially expressed between the corresponding HOIL-1-expressing controls (that is, *Ripk3*$^{-/-}$*Casp8*$^{-/-}$*Hoil-1*$^{+/-}$ and *Mlkl*$^{-/-}$*Casp8*$^{-/-}$*Hoil-1*$^{+/-}$ embryos) were excluded from the differentially expressed genes between *Ripk3*$^{-/-}$*Casp8*$^{-/-}$*Hoil-1*$^{-/-}$ and *Mlkl*$^{-/-}$*Casp8*$^{-/-}$*Hoil-1*$^{-/-}$ embryos. The resulting list of genes (33/85) was entered in the STRING software (https://string-db.org) to assess for functional enrichment in biological networks. Gene Ontology (GO) terms with false discovery rate below 1% are shown.

Flow cytometry analysis, colony-forming unit assay and macrophage culture. For phenotypic analysis, single-cell suspensions from mechanically dissociated E13.5 fetal livers or a pool of aortas (AGM region) from three embryos were stained for 30 min on ice with various antibody cocktails. The antibodies against the surface markers examined were: CD16/32, clone 93 and 2.4G2 (eBioscience, 45-0161-82 and BD553141), CD135, clone A2F10.1 (BD, 553842), Ly-6A/E, clone D7 (Sca-1) (BD, 558162), CD117 (c-Kit), clone 2B8 (BD, 560185), CD34, clone RAM34 (BD, 562608), mouse lineage cocktail, clones 17A2/RB6-8C5/RA3-6B2/Ter-119/M1/70 (Biolegend, 133313 and BD, 561301), CD16/32, clone 2.4G2 (BioXcell, CUS-HB-197), CD11b, clone M1/70 (Biolegend, 101228 and eBioscience, 15-0112-81), CD11c, clone HL3 (BD, 561241), F4/80, clone BM8 (Biolegend, 123110), GR-1, clone RB6-8C5 (Biolegend, 108416 and 108410), CD45, clone 30-F11 (Biolegend, 103128 and Biolegend, 103112), CD3ε, clone, 145-2C11 (Biolegend, 100310), B220, clone RA3-6B2, (Biolegend, 103210), CD71, clone RI7217 (Biolegend, 113807), TER-119, clone TER-119 (Biolegend, 116234) and fixable viability dye (eBioscience, 65-0864-18 and 65-0867-14). The myeloid progenitors were identified in the LK population as CD34^{+}CD16/32^{-} (CMP), CD34^{+}CD16/32^{+} (GMP); CD34^{-}CD16/32^{-} (MEP). Fluorescence minus one (FMO) was used as a gating control. For quantification of absolute number of cells, a defined number of flow cytometric reference beads (Invitrogen) were mixed with the samples before acquisition. Samples were processed either using LSR Fortessa (BD Biosciences) or sorted in a FACSAria FUSION cell sorter (BD Biosciences). Data were analysed with FlowJo 7.6.1 software (Treestar). Cytospin preparations of 10,000 cells per slide of E13.5 fetal liver homogenates were stained by May–Grünwald Giemsa staining and enucleated erythrocytes were quantified blindly as number of cells per HPF using ImageJ Software. For growth of primitive erythroid progenitor cells or all haematopoietic stem cells, 5,000 sorted Lin^{-}c-KIT^{+} E13.5 liver cells were cultured in MethoCult SF containing cytokines, including EPO (Stem Cell, M3436) or Mouse Methylcellulose Complete Media (R&D, HSC007), respectively. Colonies were enumerated after 14 days of incubation. For preparation of fetal liver-derived macrophages, equal amounts of E13.5 single cell suspensions were cultured and differentiated for 5 days in DMEM supplemented with 10% FCS plus 20% L929-conditioned medium (as a source of M-CSF) supplemented or not with the indicated inhibitors. Cells were imaged using EVOS Auto cell imaging system and viability was measured using the CellTiter-Glo Luminescent Cell Viability Assay (Promega, G7572). Alternatively, cells were stained with Hoechst dye and enumerated using Citation cell imaging platform.

Cytokine analysis. Embryo homogenates prepared as described above ('Western blot and antibodies' section) were analysed with Proteome Profiler Arrays (Mouse Angiogenesis Array, ARY015, and Mouse Cytokine array Panel A, ARY006 both R&D). ELISA kits used were the CXCL4 (R&D, DY595), CXCL11 (Abcam, ab204519), CXCL10 (R&D, DY466-05), IFN lambda 2/3 (Pbl assay science, 62830-1), IL-1β (ThermoFisher, BMS6002) and IFN-β ELISA (ThermoFisher, 424001).

Epidermal thickness quantification. Per mouse, 1–2 pieces of skin were taken and epidermal thickness was measured by microscopy using a 20× magnification. Quantification was performed by an experimenter blinded to the genotype of the mice by using the CellSens software with at least 20 measurements per mouse.

Pharmacological inhibition of RIPK1 kinase activity. Mice were fed with rodent chow containing 100 mg kg^{-1} of the RIPK1 kinase inhibitor GSK3540547A (GSK'547A) (GlaxoSmithKline LLC) starting a week before mating and kept on this diet throughout pregnancy until caesarean section at the indicated time points.

Statistics and reproducibility. Group size was determined based on preliminary datasets. Statistical significance was determined using unpaired, two-tailed parametric Student's *t*-test. One- or two-way ANOVA with Tukey's multiple comparisons test was applied. 95% Confidence interval was considered for statistics and $P < 0.05$ was considered significant. $^{*}P < 0.05$, $^{**}P < 0.01$, $^{***}P < 0.001$, $^{****}P < 0.0001$. Multiplicity-adjusted *P* values are reported for multiple comparisons. All statistical analyses were performed using Graphpad Prism 6. Statisical transformations for RNA-seq were performed with DESeq2 and adjusted *P* values used the Benjamini–Hochberg test. All in vitro experiments were performed at least twice with similar results. Unless indicated in figure legends in vivo experiments were performed with at least two embryos per genotype. At least three embryos were considered for statistical testing. The experiments were not randomized.

Reporting summary. Further information on experimental design is available in the Nature Research Reporting Summary linked to this paper.

Data availability. RNA-sequencing analysis data are available from the Sequence Read Archive (SRA) database SRP134865 (BioProject accession PRJNA437851) and comparative datasets including genes differentially regulated genes between embryo homogenates with different mutations are displayed in Supplementary Table 1.

25. Gustafsson, E., Brakebusch, C., Hietanen, K. & Fassler, R. Tie-1-directed expression of Cre recombinase in endothelial cells of embryoid bodies and transgenic mice. *J. Cell Sci.* **114**, 671–676 (2001).
26. Murphy, J. M. et al. The pseudokinase MLKL mediates necroptosis via a molecular switch mechanism. *Immunity* **39**, 443–453 (2013).
27. Newton, K., Sun, X. & Dixit, V. M. Kinase RIP3 is dispensable for normal NF-κBs, signaling by the B-cell and T-cell receptors, tumor necrosis factor receptor 1, and Toll-like receptors 2 and 4. *Mol. Cell. Biol.* **24**, 1464–1469 (2004).
28. Salmena, L. et al. Essential role for caspase 8 in T-cell homeostasis and T-cell-mediated immunity. *Genes Dev.* **17**, 883–895 (2003).
29. Kelliher, M. A. et al. The death domain kinase RIP mediates the TNF-induced NF-kappaB signal. *Immunity* **8**, 297–303 (1998).
30. Haas, T. L. et al. Recruitment of the linear ubiquitin chain assembly complex stabilizes the TNF-R1 signaling complex and is required for TNF-mediated gene induction. *Mol. Cell* **36**, 831–844 (2009).